Energy & Environmental Science

Cite this: *Energy Environ. Sci.*, 2012, **5**, 7762

www.rsc.org/ees

PAPER

Electrochemical generation of hydrogen from acetic acid using a molecular molybdenum–oxo catalyst†‡

V. Sara Thoi,[ac] Hemamala I. Karunadasa,[ac] Yogesh Surendranath,[a] Jeffrey R. Long*[ad] and Christopher J. Chang*[abc]

Received 29th February 2012, Accepted 22nd March 2012
DOI: 10.1039/c2ee21519e

We recently reported the catalytic generation of hydrogen from water mediated through the *in situ* reduction of the molybdenum(IV)–oxo complex $[(PY5Me_2)MoO]^{2+}$ (**1**; $PY5Me_2$ = 2,6-bis(1,1-bis(2-pyridyl)ethyl)pyridine) at a mercury electrode. To gain further insight into this unique molecular motif for hydrogen production, we have now examined the competence of this complex for the catalytic reduction of protons on an alternative electrode material. Herein, we demonstrate the ability of the molybdenum–oxo complex **1** to reduce protons at a glassy carbon electrode in acidic organic media, where the active catalyst is shown to be diffusing freely in solution. Cyclic and rotating disk voltammetry experiments reveal that three reductive electrochemical processes precede the catalytic generation of hydrogen, which occurs at potentials more negative than −1.25 V *vs.* SHE. Gas chromatographic analysis of the bulk electrolysis cell headspace confirms that hydrogen is generated at a Faradaic efficiency of 99%. Under pseudo-first order conditions with an acid-to-catalyst ratio of >290, a rate constant of 385 s^{-1} is calculated for the reduction of acetic acid in acetonitrile. Taken together, these data show that metal–oxo complex **1** is a competent molecular motif for catalytic generation of hydrogen from protons under soluble and diffusion-limited conditions.

[a]*Department of Chemistry and University of California, Berkeley, California 94720, USA. E-mail: jrlong@berkeley.edu; chrischang@berkeley.edu*
[b]*Howard Hughes Medical Institute, University of California, Berkeley, California 94720, USA*
[c]*Chemical Sciences Division, Lawrence Berkeley National Laboratory, Berkeley, California 94720, USA*
[d]*Materials Sciences Division, Lawrence Berkeley National Laboratory, Berkeley, California 94720, USA*

† This article was submitted following the PCET conference in October 2011.

‡ Electronic supplementary information (ESI) available. See DOI: 10.1039/c2ee21519e

Introduction

As concerns over the depletion of fossil fuels and the accumulation of their combustion byproducts escalate, the search for sustainable, economically viable energy sources have become an area of intense research. In particular, electro- and photo-catalytic methods for generating hydrogen and oxygen from water have been explored as cost-effective ways of producing a carbon-neutral fuel. While precious metals show high catalytic activity for the electro-[1–3] and photo-chemical[4–9] reduction of protons, their high cost and low terrestrial abundance make them unattractive for large-scale, distributed energy storage. Less

Broader context

The catalytic production of hydrogen from renewable resources such as water has garnered heavy interest in the search for sustainable alternative fuels. In this context we recently reported a new type of molecular motif for electrocatalytic generation of H_2 from neutral water using a high-valent molybdenum(IV)–oxo complex supported by the pentadentate ligand $PY5Me_2$. Herein, we report the investigation of this metal–oxo catalyst for hydrogen production under diffusion-limited conditions at a glassy carbon electrode using acetic acid as a proton source in acetonitrile solution. Interestingly, cyclic and rotating disc voltammetry measurements show that three reductive processes precede catalytic H_2 evolution and involve associated proton and electron transfer. Moreover, $[(PY5Me_2)MoO]^{2+}$ exhibits high stability and catalyzes hydrogen evolution at a Faradaic efficiency of 99% with a rate constant of 385 s^{-1} under pseudo-first order conditions. Taken together, our findings lend new insights into this unique molecular platform for proton reduction.

expensive heterogeneous catalysts displaying comparable activity have also been reported,[10–18] and their continued study promises to be an important area in sustainable energy research.

The potential for fine-tuning the electronic structure of molecules to optimize catalytic transformations using standard solution-based synthetic methods has also led to heavy interest in designing molecular species as catalysts for generating hydrogen and oxygen.[19–29] Advances in the area of hydrogen generation have afforded molecular catalysts that operate at moderate to low overpotentials for the reduction of protons in organic media with high rates and lifetimes.[27,30–50] The large-scale, sustainable production of hydrogen requires catalysts that function in or tolerate water as a solvent, and several examples of molecular catalysts that operate in acidic and neutral water have been reported.[15,27,30,31,39,44–47,50–54] Whereas many speculative catalytic cycles involve protonation at a low-valent metal center, protonation at a ligand has been explored as an alternative strategy towards providing a highly nucleophilic site for proton reduction,[14,41,50,55] potentially allowing for the development of more water-tolerant complexes.

We have initiated a program aimed at utilizing pyridine-based platforms for energy catalysis[43,45,47,50,56] and recently reported the electrochemical reduction of a molybdenum(IV)–oxo complex, $[(PY5Me_2)MoO](PF_6)_2$ (**1**$(PF_6)_2$; $PY5Me_2$ = 2,6-bis(1,1-bis(2-pyridyl)ethyl)pyridine), in water, which led to a rapid catalytic cycle for the cleavage of water at neutral pH to generate hydrogen under ambient conditions.[43] We speculated that reduction of **1** could render the oxo ligand more nucleophilic, where the added electrons occupied orbitals with antibonding character with respect to the metal–oxo bond.[57] Sequential proton-coupled reductions of **1** could then generate a seven-coordinate Mo(H)(OH) species poised for intramolecular H_2 elimination.[43,58] While **1** showed high activity and stability for water reduction, its significant overpotential (*ca.* 0.6 V) required the use of a mercury electrode to reduce background contributions to the measured hydrogen evolution current.[59] Cyclic voltammograms obtained with a Hg drop electrode ($A \approx 11.6 \times 10^{-3}$ cm^2) of **1**$(PF_6)_2$ in a 0.6 M pH 7 phosphate buffer solution at scan rates ranging from 0.2 to 6.5 V s^{-1} show two quasi-reversible redox couples at $E_{1/2} = -0.49$ V and -0.77 V *vs.* SHE before the onset of the catalytic current at *ca.* -0.88 V *vs.* SHE. The scan rate dependence of the peak current of the second redox event shows a linear relation for the current response to changes in scan rate (Fig. 1), revealing that the molybdenum complex is adsorbed to the Hg surface.

While the eventual utilization of a molecular proton reduction catalyst as a component of an electrochemical or photochemical water splitting device will likely require its immobilization on a surface, adsorption on Hg complicates the characterization of the catalytically active species. We therefore sought to identify conditions under which **1** is competent for catalytic hydrogen evolution without being adsorbed on the electrode. In order to evaluate the catalytic performance of **1** using a carbon electrode, we chose acetic acid as an inexpensive organic proton source with which to study the kinetics of hydrogen evolution in organic media. In this report, we present data showing that metal–oxo complex **1** is a competent molecular electrocatalyst for the reduction of protons to hydrogen under soluble and diffusion-limited conditions.

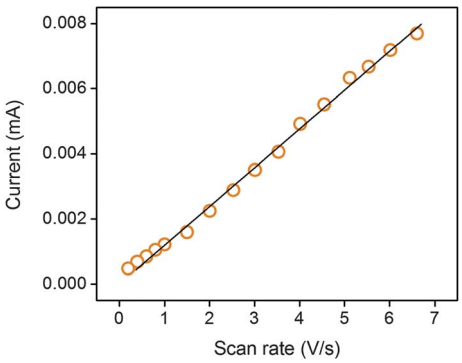

Fig. 1 Plot of the peak current *versus* the scan rate for the anodic wave of the second reduction at -0.74 V *vs.* SHE for 0.33 mM **1**$(PF_6)_2$ in a 0.6 M pH 7 phosphate buffer solution obtained on a Hg drop electrode at scan rates ranging from 0.2 V s^{-1} to 6.5 V s^{-1}. The linear fit ($y = 1.19 \times 10^{-3}x$, $R^2 = 0.996$) indicates that the reduced species is adsorbed on the Hg electrode.

Experimental section

General

The compound $[(PY5Me_2)MoO](CF_3SO_3)_2$ (**1**$(CF_3SO_3)_2$) was synthesized as previously reported.[43] Glacial acetic acid (ACS grade, VWR), acetonitrile (HPLC grade, VWR), and tetrabutylammonium hexafluorophosphate (>99.0%, Sigma-Aldrich) were used without further purification. Tetrabutylammonium benzoate (>99.0%, Sigma-Aldrich) was stored under a N_2 atmosphere and used without further purification. Benzoic acid (>99.5%, Sigma-Aldrich) was dried by heating at 100 °C at 250 mTorr for 12 h and stored under a N_2 atmosphere.

Cyclic and rotating disk electrode voltammetry

Non-aqueous electrochemical experiments were conducted under a N_2 atmosphere in a 0.1 M $(Bu_4N)PF_6$ acetonitrile solution at ambient temperature. Voltammetry and controlled-potential electrolysis experiments were carried out using a BASi Epsilon potentiostat. Rotating disk electrode voltammetry experiments were conducted with a BASi RDE-2 cell stand. All voltammetry experiments used a glassy carbon disk working electrode (3.0 mm diameter; 0.07 cm^2) and a platinum wire counter electrode. A silver wire in a glass tube with a porous Vycor tip filled with a 0.1 M $(Bu_4N)PF_6$ acetonitrile solution served as a pseudo-reference electrode. All potentials were referenced against the ferrocene/ferrocenium couple (Fc/Fc^+) as an internal standard and converted to SHE by adding 0.640 V to the measured potentials.[60,61] All electrochemical measurements were conducted without *i*R compensation. In all cases, cyclic voltammetry sweeps were recorded in quiescent solution and were initiated at the rest potential.

Chronoamperometry experiments

Potential step experiments were conducted at a rotating disk electrode at 400 rpm in the presence of 0.35 mM of **1**$(CF_3SO_3)_2$ and 5.2 mM of acetic acid in a 0.1 M $(Bu_4N)PF_6$ acetonitrile solution. The potential was stepped from 0 V to the indicated potential in Fig. S5‡. The time (τ) required for the current to

decay to within 1% of the steady-state current after a potential step is given by:[59]

$$\omega\tau\left(\frac{D}{\nu}\right)^{1/3}(0.51)^{2/3} \geq 1.3$$

where D is the diffusion coefficient, ν is the kinematic viscosity of the electrolyte solution (approximated as that of pure acetonitrile), and ω is the rotation rate. Here, D is 7.9×10^{-5} cm^2 s^{-1} (*vide infra*), ν is 0.004536 cm^2 s^{-1}, ω is 41.9 s^{-1}, and $\tau \geq 0.19$ s. The current (blue circles) plotted in Fig. S5‡ was taken at $\tau = 2.5$ s.

Controlled-potential electrolysis and gas chromatographic analysis

Controlled-potential electrolysis was conducted using a custom-made air-tight glass double compartment cell separated by a glass frit. The working compartment was fitted with a glassy carbon rod working electrode (2.5 mm diameter, 2 cm length) and a Ag/AgNO$_3$ reference electrode. The auxiliary compartment was fitted with a Pt gauze electrode. The working compartment was filled with 50 mL of 35 mM acetic acid in a 0.1 M $(Bu_4N)PF_6$ acetonitrile solution, while the auxiliary compartment was filled with 70 mL of 0.1 M $(Bu_4N)PF_6$ acetonitrile solution, resulting in equal solution levels in both compartments. Solution diffusion across the glass frit was slow under static pressure. Both compartments were sparged for 15 min with N_2 and cyclic voltammograms were recorded as controls. Catalyst **1**$(CF_3SO_3)_2$ (0.1 mM) was then added and a cyclic voltammogram was recorded. Electrolysis was conducted for 1 h and the headspace was subjected to gas chromatographic analysis. An Agilent 490-GC Micro-Gas Chromatograph with a molecular sieve column and heated syringe injector was used for product detection. The column was heated to 80 °C under Ar gas flow and an average sample volume of 200 nL was injected onto the column. The integrated area of the H_2 peak was compared to a calibration curve (*vide infra*) to calculate the moles of H_2 generated. To determine the Faradaic efficiency, this value was divided by the theoretical yield of hydrogen expected based on the charge passed over the course of the experiment.

Calibration. Using the double-compartment cell described above, the working compartment was filled with 50 mL of 35 mM acetic acid in a 0.1 M $(Bu_4N)PF_6$ acetonitrile solution, while the auxiliary compartment was filled with 70 mL of a 0.1 M $(Bu_4N)PF_6$ acetonitrile solution. Both compartments were sparged thoroughly with N_2 and sealed. A 5 mL aliquot of the headspace was removed and replaced with 5 mL of CH_4. Aliquots of 0.5, 1, 2, and 3 mL of H_2 were introduced to the headspace and the solution was allowed to stir for at least 30 min. A sample of the headspace was injected into the gas chromatograph and the ratio of CH_4 and H_2 was taken as points on a calibration curve (Fig. S7‡).

Results and discussion

Cyclic voltammetry studies

In acetonitrile solution at a glassy carbon electrode, the molybdenum(IV)–oxo complex displays a rich reductive electrochemistry without adsorbing to the electrode surface. As reported previously,[43] the cyclic voltammogram of 0.7 mM **1**$(CF_3SO_3)_2$ in a 0.1 M $(Bu_4N)PF_6$ acetonitrile solution at a glassy carbon disk electrode, at a scan rate of 0.1 V s^{-1}, shows reversible $[(PY5Me_2)MoO]^{2+/1+}$ and $[(PY5Me_2)MoO]^{2+/3+}$ redox couples at $E_{1/2} = -0.84$ and 1.41 V *vs.* SHE, respectively. Scanning to cathodic potentials beyond the first reversible reduction reveals an irreversible redox event at a cathodic peak potential of $E_{p,c} = -1.24$ V followed by a reversible couple at $E_{1/2} = -1.55$ V *vs.* SHE.

Since reduction of the Mo center is expected to increase the basicity of the oxo ligand, we hypothesized that the irreversibility of the second wave may be due to inefficient proton transfer. To examine this hypothesis, cyclic voltammograms were collected in the presence of stoichiometric and substoichiometric amounts of acid. A cyclic voltammogram of 0.5 mM **1**$(CF_3SO_3)_2$ in the presence of 0.25 mM of acetic acid (0.5 equiv.) shows growth of two new reversible reductive events at $E_{1/2} = -0.73$ and -1.08 V *vs.* SHE, with concomitant attenuation of the reductive events at $E_{1/2} = -0.84$ and $E_{p,c} = -1.24$ V *vs.* SHE (Fig. 2). In the presence of one equivalent of acetic acid, the cyclic voltammogram of **1**$(CF_3SO_3)_2$ displays three reversible reductive processes at $E_{1/2} = -0.73$, -1.08, and -1.55 V *vs.* SHE, all of which are diffusion-limited, as evidenced by their square root dependence on the scan rate (Fig. 3). Thus, we postulate that in the absence of acid, the second reduction event is accompanied by adventitious protonation from trace water or acidic functionality on the glassy carbon surface. This would result in sluggish back proton transfer kinetics that would inhibit the return oxidation reaction and give rise to an irreversible wave. In contrast, in the presence of submillimolar concentrations of acid, both forward and reverse proton transfers are rapid, resulting in three reversible redox waves. The diffusion-limited nature of these waves contrasts with what is observed for the compound in water on a mercury cathode, where reduction leads to adsorption on the electrode surface before the onset of catalytic hydrogen evolution (Fig. 1).[29]

Catalytic hydrogen production can also be achieved with the molybdenum(IV)–oxo complex in acetonitrile by supplying an excess of organic acid as a proton source. Addition of 50 equiv. of acetic acid (35 mM) to a solution containing 0.7 mM

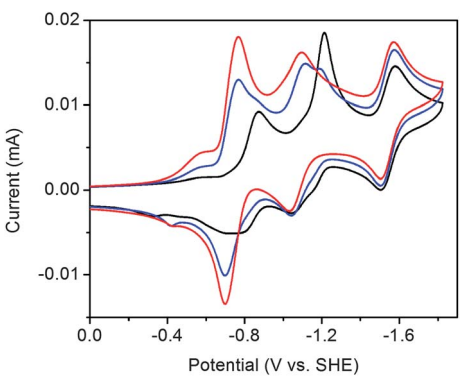

Fig. 2 Cyclic voltammograms of 0.5 mM **1**$(CF_3SO_3)_2$ in a 0.1 M of $(Bu_4N)PF_6$ acetonitrile solution with 0 mM (black), 0.25 mM (blue, 0.5 equiv.), and 0.5 mM (red, 1 equiv.) of acetic acid at a glassy carbon disc electrode and a scan rate of 0.1 V s^{-1}. In the presence of a proton source, all three reductive processes are reversible and diffusion-limited.

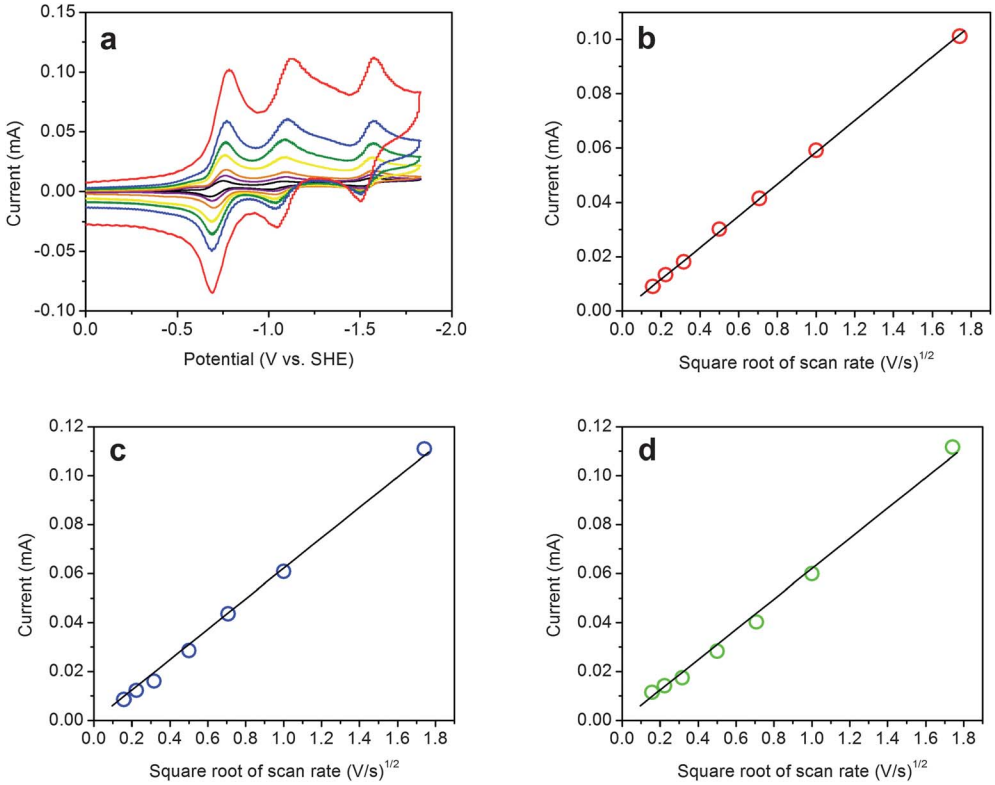

Fig. 3 (a) Cyclic voltammograms of 0.5 mM **1**$(CF_3SO_3)_2$ in a 0.1 M $(Bu_4N)PF_6$ acetonitrile solution in the presence of one equivalent of acetic acid, and plots of the current *versus* the square root of the scan rate for the (b) first (red, $R^2 = 1.00$), (c) second (blue, $R^2 = 0.999$), and (d) third (green, $R^2 = 0.994$) reductions at a glassy carbon disc electrode for scan rates from 0.025 to 3.03 V s^{-1}. The linear fits to the data indicate that the reduced species are freely diffusing in solution at all potentials in the presence of a proton source.

1$(CF_3SO_3)_2$ leads to a positive shift in the reduction potentials, with the first redox couple occurring at $E_{1/2} = -0.57$ V followed by a reduction event at $E_{1/2} = -0.80$ V *vs.* SHE (Fig. 4). As shown in Fig. 5, the magnitude of the positive shift varies as a function of acid strength with the most positive shifts occurring with stronger acids, suggesting protonation is associated with electron transfer. The proton-coupled nature of these reduction events is further substantiated by cyclic voltammograms of 0.5 mM **1**$(CF_3SO_3)_2$ with varying ratios of benzoic acid and tetrabutylammonium benzoate. Relative to a 1 : 1 ratio of benzoic acid to tetrabutylammonium benzoate, the first and second reduction events shift by 90 mV and 56 mV, respectively, in the presence of a 10 : 1 ratio of benzoic acid to tetrabutylammonium benzoate (Fig. S1‡), though further studies are necessary to determine the cause of these shifts.

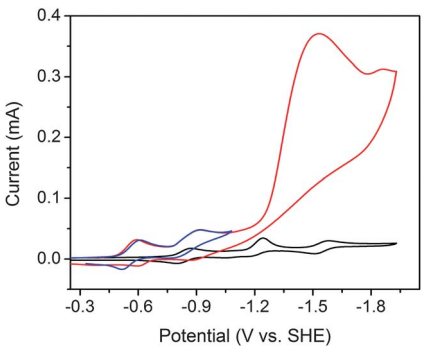

Fig. 4 Cyclic voltammograms of 0.7 mM **1**$(CF_3SO_3)_2$ in a 0.1 M $(Bu_4N)PF_6$ acetonitrile solution at a glassy carbon disk electrode at a scan rate of 0.1 V s^{-1} in the absence (black line) and presence (blue and red lines) of 35 mM acetic acid. Blue and red lines indicate initial and subsequent scans, respectively.

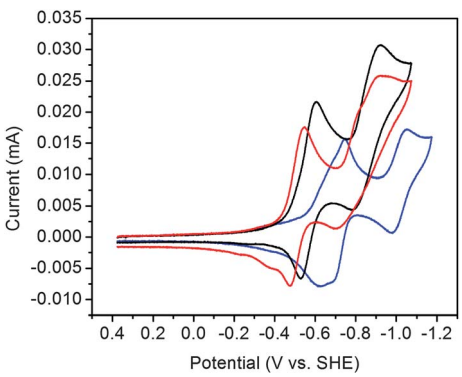

Fig. 5 Cyclic voltammograms of 0.5 mM **1**$(CF_3SO_3)_2$ in a 0.1 M of $(Bu_4N)PF_6$ acetonitrile solution with 35 mM benzoic acid (red, pK_a 20.7), acetic acid (black, pK_a 22.3) and phenol (blue, pK_a 27.2) at a glassy carbon disc electrode and a scan rate of 0.1 V s^{-1}. The stronger acids lead to a more positive shift in the two precatalytic reduction potentials, suggesting protonation is coupled with electron transfer. Reported pK_a values in acetonitrile were obtained from ref. 61.

In the presence of excess acetic acid, scanning more negative than the second reduction event results in a sharp increase in current, indicative of catalytic proton reduction with an onset potential of −1.25 V *vs.* SHE. This catalytic current peaks at $E_p = -1.60$ V *vs.* SHE, with half the maximum current attained at a potential of $E_{p,½} = -1.40$ V. Evans[61] and Artero[62] reported the thermodynamic potential (E°) for the reduction of acetic acid in acetonitrile as −0.82 and −0.59 V *vs.* SHE, respectively. As such, the $E_{p,½}$ of −1.40 V for the reduction of acetic acid by **1**$(CF_3SO_3)_2$ yields an overpotential of 580 and 810 mV based on these two studies, respectively.[61,62] For comparison, direct reduction of 35 mM acetic acid in a 0.1 M $(Bu_4N)PF_6$ acetonitrile solution at a glassy carbon disk electrode occurs at an onset potential of *ca.* −1.50 V with $E_p = -2.00$ V and $E_{p,½} = -1.73$ V *vs.* SHE (Fig. S2‡). Further additions of acid to a solution containing 0.7 mM **1**$(CF_3SO_3)_2$ lead to higher current enhancements and a positive shift of the onset potential (Fig. 6). Plots of the peak currents for the two precatalytic waves as well as for the catalytic current *versus* the square root of the scan rate show linear relationships, indicating that the redox-active species are freely diffusing in solution (Fig. S3‡). The catalytic nature of the peak at −1.60 V *vs.* SHE is established by passing *ca.* 25 equiv. of charge during a controlled-potential electrolysis conducted in a double-compartment cell, where the potential is held at −1.6 V *vs.* SHE for 1 h (Fig. 7 and S4‡). Analysis of the electrolysis cell headspace by gas chromatography confirms the production of hydrogen with a Faradaic efficiency of 99%.

After establishing that **1** can catalytically reduce protons in acidic organic media, we turned our attention to the kinetics of this process. Using the method described by DuBois and co-workers,[46,63] the following equation allows us to determine the observed rate constant for catalytic turnover under conditions of negligible acid consumption over the course of the CV sweep.

$$\frac{i_c}{i_p} = \frac{n}{0.4463}\sqrt{\frac{RTk_{obs}}{Fv}} \quad (1)$$

Here, i_p is the peak current of the third reduction in the absence of acid, i_c is the catalytic peak current plateau, n is the number of electrons involved in each catalytic turnover ($n = 2$), R is the universal gas constant (8.314 J K^{-1} mol^{-1}), T is temperature (K), F is the Faraday constant (96 485 A s mol^{-1}), v is the scan rate (0.05 V s^{-1}), and k_{obs} is the observed rate constant (s^{-1}). Importantly, the above equation is accurate in the limit of negligible acid consumption. Under such conditions, the CV waveform is expected to exhibit an S-shaped catalytic wave with a well-defined plateau and overlapping forward and reverse scans. In our system, even at very high acid concentrations relative to catalyst (excess factor >290), we observe peak-shaped catalytic waves displaying appreciable current hysteresis between forward and return scans. This behavior is indicative of significant substrate consumption over the course of the CV scan. Notwithstanding, we utilize eqn (2) to extract *lower limit* estimates of k_{obs} at high acid concentration and acknowledge that future studies are necessary to derive an accurate electrochemical rate law for hydrogen evolution. After subtracting the current from the direct reduction of protons at the glassy carbon electrode, a plot of i_c/i_p against acid concentration (Fig. 8) exhibits

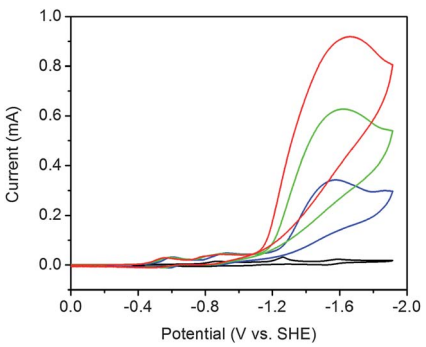

Fig. 6 Cyclic voltammograms of 0.5 mM **1**$(CF_3SO_3)_2$ in a 0.1 M $(Bu_4N)PF_6$ acetonitrile solution obtained at a glassy carbon disk electrode at a scan rate of 0.1 V s^{-1} in the presence of 0 (black line), 35 mM (blue), 70 mM (green), and 105 mM (red) acetic acid.

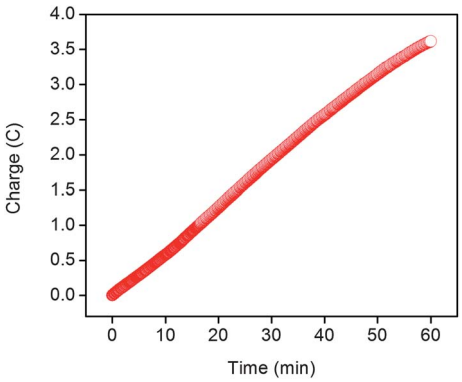

Fig. 7 Charge build-up *versus* time for 0.1 mM **1**$(CF_3SO_3)_2$ in a 0.1 M $(Bu_4N)PF_6$ acetonitrile solution and 17 mM of acetic acid at a glassy carbon rod electrode operating at a potential of −1.6 V *vs.* SHE for 1 h. Background activity of direct proton reduction at the electrode has been subtracted from the data.

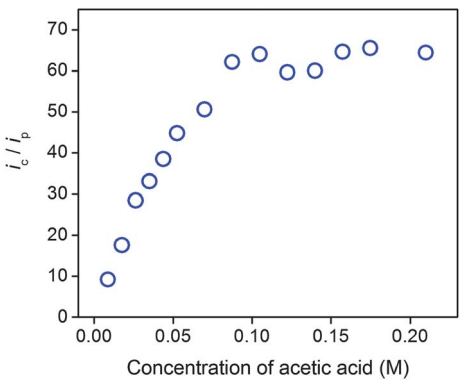

Fig. 8 A plot of i_c/i_p *versus* the concentration of acetic acid taken at 0.050 V s^{-1} for 0.35 mM **1**$(CF_3SO_3)_2$ in a 0.1 M $(Bu_4N)PF_6$ acetonitrile solution. At low acid concentrations, i_c/i_p varies linearly against the concentration of acetic acid; however, i_c/i_p exhibits plateau-like behavior at high acid concentration (>0.1 M). The rate constant is determined at this acid-independent region to be 385 s^{-1}, according to eqn (2). Current from direct reduction of acetic acid at the glassy carbon electrode has been subtracted from the data and the catalytic peak current plateau, i_c, was taken at the catalytic peak current as an approximation in our calculations.

two regions. At acid concentrations below 0.1 M, i_c/i_p varies linearly with the acid concentration. However, at acid concentrations above 0.1 M, i_c/i_p becomes independent of the acid concentration. Using the average i_c/i_p value observed in the acid-independent region, we estimate a k_{obs} of 385 s^{-1}.

Rotating disk electrode voltammetry (RDEV) studies

A rotating disk electrode is utilized to probe the hydrodynamics of the system. Rotating the electrode at a fixed rate, ω (rpm), transports the dissolved catalyst in the bulk solution to the electrode at a fixed rate, creating a steady-state concentration profile and therefore a steady-state current at the electrode surface. Fig. 9a shows the steady-state RDE voltammograms of **1**$(CF_3SO_3)_2$ obtained for different rotation rates at a scan rate of 0.025 V s^{-1} and exhibits three current plateaus indicative of three distinct electrochemical reductions. Similar to the cyclic voltammetry results, the addition of 50 equiv. of acetic acid (17 mM) generates two current plateaus, followed by a sharp increase in the current response which levels at a value approximately 10 times higher than the steady state current obtained from the catalyst alone at the same potential of −1.6 V *vs.* SHE. Half of the steady state current is achieved at a potential of −1.4 V *vs.* SHE, yielding an overpotential of 580 mV and 810 mV, depending on the E° value for hydrogen evolution (*vide supra*), for the reduction of 35 mM acetic acid.[62] The RDE voltammogram is also consistent with three electrochemical reductions preceding the catalytic generation of hydrogen. The variation of the steady state current as a function of the rotation rate, given by the Levich relation, shown below in eqn (3), is used to calculate the diffusion coefficient, D, for **1** in the electrolyte solution (Fig. 9b).

$$J_L = \frac{0.62nFD^{2/3}[\mathbf{1}]\omega^{1/2}}{\nu^{1/6}} \quad (2)$$

In the absence of acid, the Levich plot of the current density (J_L) at approximately −1.8 V *vs.* SHE varies linearly as a function of $\omega^{1/2}$. A linear fit through the origin gives a slope of 1.34×10^{-4} A $s^{1/2}$ ($R^2 = 1.00$). Assuming that the kinematic viscosity (ν) of the electrolyte solution is the same as that of pure acetonitrile (0.00435 cm^2 s^{-1}), and using $n = 1$ as the number of electrons transferred in the third reduction event, a diffusion coefficient of $D = 7.9 \times 10^{-5}$ cm^2 s^{-1} is calculated. Upon addition of 50 equiv. of acetic acid, the Levich plot deviates from linearity at rotation rates greater than 1600 rpm, suggesting the onset of kinetic limitations.[64]

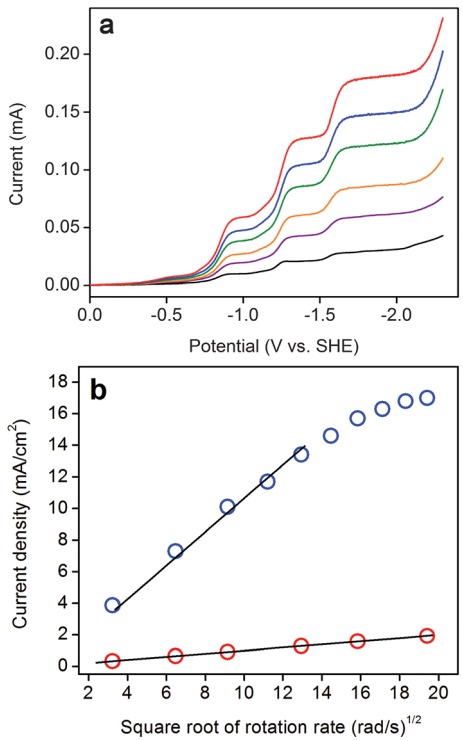

Fig. 9 (a) RDE voltammograms of 0.36 mM **1**$(CF_3SO_3)_2$ in a 0.1 M $(Bu_4N)PF_6$ acetonitrile solution with rotation rates of 100 (black), 400 (orange), 800 (green), 1600 (yellow), 2400 (blue), and 3600 rpm (red) and a scan rate of 0.025 V s^{-1}. (b) Levich plot of the current density at −1.8 V *versus* the square root of the rotation rate in the absence (red circles) and in the presence (blue circles) of 17 mM acetic acid. Linear fits to the data (black lines) show that the current density is diffusion-limited for all rotation rates in the absence of acid ($y = 0.0998x$, $R^2 = 1.000$), and for rotation rates below *ca.* 1600 rpm in the presence of acid ($y = 1.06x$, $R^2 = 0.989$).

Potential-dependent "apparent rate" of hydrogen production

In order to evaluate the performance of **1** for producing hydrogen from acetic acid at various overpotentials and to provide a point of reference for comparison with other molecular proton reduction catalysts that use the same acid source, we use a recently described method[65–70] to determine apparent rates of proton reduction, defined as the number of turnovers the catalyst performs during the period it is at the electrode surface. This method normalizes for the diffusion of the molecular catalyst to the electrode surface at a particular rotation rate by dividing the catalytic current by the current generated by the catalyst alone at the same potential.

To confirm that the conditions used in the RDEV experiments create steady-state currents, chronoamperometry experiments are performed using the rotating disk electrode of a 0.1 M $(Bu_4N)PF_6$ acetonitrile solution containing **1**$(CF_3SO_3)_2$ (0.34 mM) and excess acetic acid (5.2 mM). Here, potential steps from 0 to potentials ranging from −0.29 to −2.09 V *vs.* SHE are measured at a rotation rate of 400 rpm. Upon application of a potential step, the current–time profile decays to within 1% of the steady-state current at time, $\tau \geq 0.19$ s.[59] As shown in Fig. S5‡, the steady-state current obtained through the application of potential steps matches the steady-state current determined through RDEV performed at the same scan rate, rotation rate, and concentrations of **1**$(CF_3SO_3)_2$ and acetic acid. This result confirms that a rotation rate of 400 rpm is sufficient for obtaining a steady state current under these conditions.

We next evaluated the parameter $n_{app}(E)$, defined as the apparent number of electrons delivered from the catalyst to the substrate, at a specific applied potential and rotation rate, during the time period that the molecular catalyst is at the electrode.[59,70] At a given potential where proton reduction catalysis occurs, and at a fixed rotation rate where steady-state current is achieved, $n_{app}(E)$ is defined as:

$$n_{app}(E) = \frac{nJ_c(E)}{J_p} \quad (3)$$

Here, n is the number of electrons involved in the reduction of **1** in the absence of acid ($n = 1$), $J_c(E)$ is the catalytic current density at potential E, and J_p is the current density generated by **1** in the absence of acid at −1.6 V *vs.* SHE. The values for n_{app} at various potentials are shown in Fig. 10a. At potentials where contributions from direct reduction of acetic acid at the glassy carbon electrode are observed (potentials more negative than −1.5 V *vs.* SHE), the background current is subtracted from the data. We note that this procedure gives a lower bound for n_{app} at these potentials, because the current generated by direct reduction of protons at the electrode is not limited by the diffusion of a molecular catalyst to the electrode surface. Similar to the results found in the kinetic studies using cyclic voltammetry, n_{app} is independent of acid concentration above *ca.* 0.1 M and exhibits plateau-like behavior (Fig. 10b). In this acid-independent region and at an applied potential of −1.6 V *vs.* SHE, n_{app} is approximately 16. To convert from the "apparent number of electrons" to an "apparent turnover rate" (TOR) defined as the number of H_2 molecules produced by the catalyst during the time period it is at the electrode, the Faradaic efficiency of the catalyst (determined through bulk electrolysis) is taken into account as shown in the following equation:

$$\text{TOR} = \frac{n_{app}(E)}{n_{cat}} f \quad (4)$$

Here, f describes the Faradaic efficiency at −1.6 V, and n_{cat} is the number of electrons required to produce a molecule of hydrogen ($n_{cat} = 2$) (Fig. S6‡). This analysis gives an apparent TOR of *ca.* 8 s^{-1} at an applied potential of −1.6 V *vs.* SHE and at acid concentrations above 0.1 M. We note that, as discussed previously,[70] n_{app} and the TOR are not true kinetic measurements but only reference values for comparison with other molecular catalysts that reduce acetic acid to hydrogen under identical conditions.

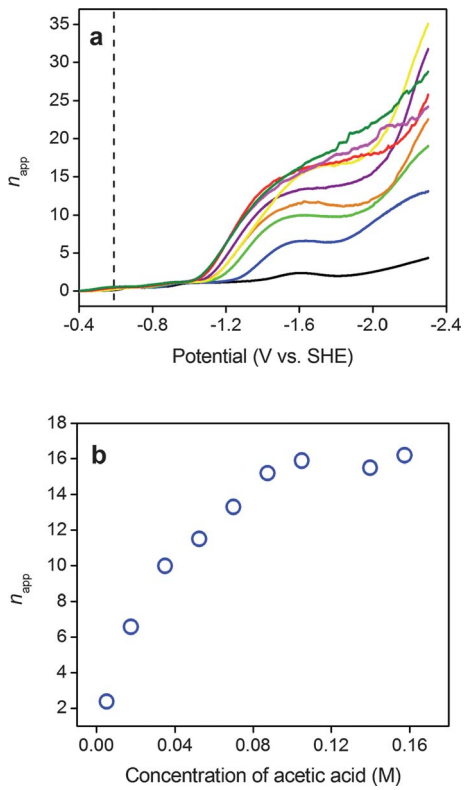

Fig. 10 (a) The apparent rate of electron delivery, n_{app}, for 0.35 mM **1**$(CF_3SO_3)_2$ in a 0.1 M $(Bu_4N)PF_6$ acetonitrile solution in the presence of 5.2 mM (black), 17 mM (blue), 35 mM (green), 52 mM (orange), 70 mM (purple), 87 mM (yellow), 105 mM (red), 140 mM (olive), and 157 mM (magenta) of acetic acid, at a scan rate of 0.025 V s^{-1} and a rotation rate of 400 rpm, at a glassy carbon disk electrode. The dotted vertical line at −0.59 V *vs.* SHE indicates the thermodynamic potential for the reduction of acetic acid to H_2 in acetonitrile.[62] (b) n_{app} plotted against concentration of acid. At acid concentrations above 0.1 M, n_{app} is independent of acid concentration and exhibits plateau-like behavior. Current from direct reduction of acetic acid at the glassy carbon electrode has been subtracted from the data.

The direct comparison of molecular catalysts for proton reduction remains a challenge, because the activities for different catalysts have usually been assessed under very different conditions. In organic media, acids are typically chosen such that the thermodynamic potential for acid reduction is close to the $E_{p,½}$ of the catalytic current (the potential where the catalytic current reaches half its maximum value), resulting in a low overpotential for proton reduction with respect to the specific acid chosen in the study.[61,62] Low overpotentials have been achieved for catalytic nickel[24,25,27,46,71] and cobalt complexes,[72] using acids such as triflic,[71] triethylammonium chloride,[35] trifluoroacetic[45,73] and *p*-toluenesulfonic acid.[38] Restricting the discussion to catalysts evaluated under similar conditions, (*i.e.*, under sufficiently high acid concentrations where the catalytic current is independent of the acid concentration), DuBois and co-workers have reported a series of Ni bis(diphosphine) complexes that utilize the secondary coordination sphere to enhance the reduction of organic acids to H_2 in acetonitrile.[24,25,27,46] Using protonated dimethylformamide and anilinium salts in acetonitrile with small amounts of water, Ni bis(diphospine) complexes containing pendant amines as proton relays can generate H_2 with turnover frequencies ranging from 15 s^{-1} to 106 000 s^{-1} with overpotentials from 220 mV to 625 mV,[27,46] based on E° values reported by Evans.[61] Mo–S dimers and oxothiomolybdenum wheel-shaped clusters can reduce a range of organic acids with overpotentials of ~100 mV and a rate constant of ~1.5 s^{-1}.[41,55] While the overpotential for proton reduction by **1** is significant (580 mV[61] or 810 mV,[62] depending on the E° value employed), a rate constant of 385 s^{-1} is observed with acetic acid, an inexpensive acid currently produced industrially on a large scale.[74] More importantly, these data show that successive reductions and protonations of a metal–oxo complex generate a catalyst competent for hydrogen evolution in acidic organic media and provide a baseline for systematic improvements.

Conclusions

Voltammetry and controlled-potential electrolysis studies using carbon electrodes show that the electrochemical reduction of the molecular molybdenum–oxo complex, $[(PY5Me_2)MoO]^{2+}$, forms a competent catalyst for the reduction of protons in acidic organic media with a Faradaic efficiency of 99%. Importantly,

cyclic and rotating disk electrode voltammetry indicate that the active catalyst is freely diffusing in solution, and that three electrochemical reductive processes precede the onset of catalytic proton reduction. At acid concentration in excess of 0.1 M, the rate constant, k_{obs}, for hydrogen evolution is estimated to be 385 s^{-1}. An "apparent turnover rate" for the reduction of acetic acid in acetonitrile by **1** of 8 s^{-1} at −1.6 V *vs.* SHE is also calculated as a metric for comparison to similar catalysts evaluated under identical conditions. Ongoing efforts are focused on decreasing the overpotential for proton reduction by **1** and related polypyridyl systems, with particular interest in developing catalysts that are compatible with aqueous media.

Acknowledgements

The synthetic portion of this work was supported by DOE/LBNL Grant 403801 (C.J.C.). The electrochemical studies were funded by the Helios Solar Energy Research Center (SERC, 51HE112B), which is supported by the Director, Office of Science, Office of Basic Energy Sciences, Department of Energy, under Contract No. DE-AC02-05CH11231 (C.J.C.). In addition, the contributions of J.R.L. to this work were supported by NSF grant CHE-1111900. We thank Prof. T. D. Tilley for use of his laboratory's rotating disk electrode as well as Dr C. C. L. McCrory and Dr J. Yang for helpful discussions. We also acknowledge Ms A. T. Chantarojsiri for experimental assistance and helpful discussions. V.S.T. thanks the National Science Foundation for a graduate fellowship, and Y.S. acknowledges the Miller Institute for Basic Research for a postdoctoral fellowship. C.J.C. is an Investigator with the Howard Hughes Medical Institute.

References

1 C. S. C. Bose and K. Rajeshwar, *J. Electroanal. Chem.*, 1992, **333**, 235–256.
2 J. P. Collman, Y. Ha, P. S. Wagenknecht, M. A. Lopez and R. Guilard, *J. Am. Chem. Soc.*, 1993, **115**, 9080–9088.
3 C. Caix, S. Chardon-Noblat, A. Deronzier, J.-C. Moutet and S. Tingry, *J. Organomet. Chem.*, 1997, **540**, 105–111.
4 U. Kölle and M. Grätzel, *Angew. Chem., Int. Ed. Engl.*, 1987, **26**, 567–570.
5 J. I. Goldsmith, W. R. Hudson, M. S. Lowry, T. H. Anderson and S. Bernhard, *J. Am. Chem. Soc.*, 2005, **127**, 7502–7510.
6 A. J. Esswein and D. G. Nocera, *Chem. Rev.*, 2007, **107**, 4022–4047.
7 L. L. Tinker, N. D. McDaniel, P. N. Curtin, C. K. Smith, M. J. Ireland and S. Bernhard, *Chem.–Eur. J.*, 2007, **13**, 8726–8732.
8 P. Du, K. Knowles and R. Eisenberg, *J. Am. Chem. Soc.*, 2008, **130**, 12576–12577.
9 L. L. Tinker and S. Bernhard, *Inorg. Chem.*, 2009, **48**, 10507–10511.
10 S. Trasatti, *J. Electroanal. Chem.*, 1972, **39**, 163–184.
11 B. E. Conway, L. Bai and M. A. Sattar, *Int. J. Hydrogen Energy*, 1987, **12**, 607–621.
12 A. K. Cheong, A. Lasia and J. Lessard, *J. Electrochem. Soc.*, 1993, **140**, 2721–2725.
13 B. Hinnemann, P. G. Moses, J. Bonde, K. P. Jørgensen, J. H. Nielsen, S. Horch, I. Chorkendorff and J. K. Nørskov, *J. Am. Chem. Soc.*, 2005, **127**, 5308–5309.
14 T. F. Jaramillo, J. Bonde, J. Zhang, B.-L. Ooi, K. Andersson, J. Ulstrup and I. Chorkendorff, *J. Phys. Chem. C*, 2008, **112**, 17492–17498.
15 T. R. Cook, D. K. Dogutan, S. Y. Reece, Y. Surendranath, T. S. Teets and D. G. Nocera, *Chem. Rev.*, 2010, **110**, 6474–6502.
16 Y. Li, H. Wang, L. Xie, Y. Liang, G. Hong and H. Dai, *J. Am. Chem. Soc.*, 2011, **133**, 7296–7299.
17 S. Y. Reece, J. A. Hamel, K. Sung, T. D. Jarvi, A. J. Esswein, J. J. H. Pijpers and D. G. Nocera, *Science*, 2011, **334**, 645–648.
18 D. Merki, S. Fierro, H. Vrubel and X. Hu, *Chem. Sci.*, 2011, **2**, 1262–1267.
19 D. J. Evans and C. J. Pickett, *Chem. Soc. Rev.*, 2003, **32**, 268–275.
20 M. W. Kanan and D. G. Nocera, *Science*, 2008, **321**, 1072–1075.
21 F. Gloaguen and T. B. Rauchfuss, *Chem. Soc. Rev.*, 2009, **38**, 100–108.
22 J. J. Concepcion, J. W. Jurss, M. K. Brennaman, P. G. Hoertz, A. O. v. T. Patrocinio, N. Y. Murakami Iha, J. L. Templeton and T. J. Meyer, *Acc. Chem. Res.*, 2009, **42**, 1954–1965.
23 G. C. Dismukes, R. Brimblecombe, G. A. N. Felton, R. S. Pryadun, J. E. Sheats, L. Spiccia and G. F. Swiegers, *Acc. Chem. Res.*, 2009, **42**, 1935–1943.
24 M. Rakowski Dubois and D. L. Dubois, *Acc. Chem. Res.*, 2009, **42**, 1974–1982.
25 M. Rakowski DuBois and D. L. DuBois, *Chem. Soc. Rev.*, 2009, **38**, 62–72.
26 M. W. Kanan, J. Yano, Y. Surendranath, M. Dincă, V. K. Yachandra and D. G. Nocera, *J. Am. Chem. Soc.*, 2010, **132**, 13692–13701.
27 M. L. Helm, M. P. Stewart, R. M. Bullock, M. R. DuBois and D. L. DuBois, *Science*, 2011, **333**, 863–866.
28 D. J. Wasylenko, C. Ganesamoorthy, J. Borau-Garcia and C. P. Berlinguette, *Chem. Commun.*, 2011, **47**, 4249–4251.
29 D. E. Polyansky, J. T. Muckerman, J. Rochford, R. Zong, R. P. Thummel and E. Fujita, *J. Am. Chem. Soc.*, 2011, **133**, 14649–14665.
30 R. M. Kellett and T. G. Spiro, *Inorg. Chem.*, 1985, **24**, 2373–2377.
31 P. Connolly and J. H. Espenson, *Inorg. Chem.*, 1986, **25**, 2684–2688.
32 I. Bhugun, D. Lexa and J.-M. Savéant, *J. Am. Chem. Soc.*, 1996, **118**, 3982–3983.
33 F. Gloaguen, J. D. Lawrence and T. B. Rauchfuss, *J. Am. Chem. Soc.*, 2001, **123**, 9476–9477.
34 S. Ott, M. Borgström, M. Kritikos, R. Lomoth, J. Bergquist, B. Åkermark, L. Hammarström and L. Sun, *Inorg. Chem.*, 2004, **43**, 4683–4692.
35 M. Razavet, V. Artero and M. Fontecave, *Inorg. Chem.*, 2005, **44**, 4786–4795.
36 L. Sun, B. Åkermark and S. Ott, *Coord. Chem. Rev.*, 2005, **249**, 1653–1663.
37 C. Baffert, V. Artero and M. Fontecave, *Inorg. Chem.*, 2007, **46**, 1817–1824.
38 X. Hu, B. S. Brunschwig and J. C. Peters, *J. Am. Chem. Soc.*, 2007, **129**, 8988–8998.
39 O. Pantani, E. Anxolabéhère-Mallart, A. Aukauloo and P. Millet, *Electrochem. Commun.*, 2007, **9**, 54–58.
40 M. H. Cheah, C. Tard, S. J. Borg, X. Liu, S. K. Ibrahim, C. J. Pickett and S. P. Best, *J. Am. Chem. Soc.*, 2007, **129**, 11085–11092.
41 B. Keita, S. Floquet, J.-F. Lemonnier, E. Cadot, A. Kachmar, M. Benard, M.-M. Rohmer and L. Nadjo, *J. Phys. Chem. C*, 2008, **112**, 1109–1114.
42 J. L. Dempsey, B. S. Brunschwig, J. R. Winkler and H. B. Gray, *Acc. Chem. Res.*, 2009, **42**, 1995–2004.
43 H. I. Karunadasa, C. J. Chang and J. R. Long, *Nature*, 2010, **464**, 1329–1333.
44 L. A. Berben and J. C. Peters, *Chem. Commun.*, 2010, **46**, 398–400.
45 J. P. Bigi, T. E. Hanna, W. H. Harman, A. Chang and C. J. Chang, *Chem. Commun.*, 2010, **46**, 958–960.
46 U. J. Kilgore, J. A. S. Roberts, D. H. Pool, A. M. Appel, M. P. Stewart, M. R. DuBois, W. G. Dougherty, W. S. Kassel, R. M. Bullock and D. L. DuBois, *J. Am. Chem. Soc.*, 2011, **133**, 5861–5872.
47 Y. Sun, J. P. Bigi, N. A. Piro, M. L. Tang, J. R. Long and C. J. Chang, *J. Am. Chem. Soc.*, 2011, **133**, 9212–9215.
48 M. Beyler, S. Ezzaher, M. Karnahl, M.-P. Santoni, R. Lomoth and S. Ott, *Chem. Commun.*, 2011, **47**, 11662–11664.
49 W. R. McNamara, Z. Han, P. J. Alperin, W. W. Brennessel, P. L. Holland and R. Eisenberg, *J. Am. Chem. Soc.*, 2011, **133**, 15368–15371.
50 H. I. Karunadasa, E. Montalvo, Y. Sun, M. Majda, J. R. Long and C. J. Chang, *Science*, 2012, **335**, 698–702.
51 P. V. Bernhardt and L. A. Jones, *Inorg. Chem.*, 1999, **38**, 5086–5090.
52 B. J. Fisher and R. Eisenberg, *J. Am. Chem. Soc.*, 1980, **102**, 7361–7363.
53 J. P. Collin, A. Jouaiti and J. P. Sauvage, *Inorg. Chem.*, 1988, **27**, 1986–1990.

54 B. D. Stubbert, J. C. Peters and H. B. Gray, *J. Am. Chem. Soc.*, 2011, **133**, 18070–18073.
55 A. M. Appel, D. L. DuBois and M. Rakowski DuBois, *J. Am. Chem. Soc.*, 2005, **127**, 12717–12726.
56 H. S. Soo, A. C. Komor, A. T. Iavarone and C. J. Chang, *Inorg. Chem.*, 2009, **48**, 10024–10035.
57 H. B. Gray and C. R. Hare, *Inorg. Chem.*, 1962, **1**, 363–368.
58 E. J. Sundstrom, X. Yang, V. S. Thoi, H. I. Karunadasa, C. J. Chang, J. R. Long and M. Head-Gordon, *J. Am. Chem. Soc.*, 2012, **134**, 5233–5242.
59 A. J. F. Bard and R. Larry, *Electrochemical Methods: Fundamentals and Applications*, John Wiley & Sons, New York, 2001.
60 N. G. Connelly and W. E. Geiger, *Chem. Rev.*, 1996, **96**, 877–910.
61 G. A. N. Felton, R. S. Glass, D. L. Lichtenberger and D. H. Evans, *Inorg. Chem.*, 2006, **45**, 9181–9184.
62 V. Fourmond, P.-A. Jacques, M. Fontecave and V. Artero, *Inorg. Chem.*, 2010, **49**, 10338–10347.
63 D. H. Pool and D. L. DuBois, *J. Organomet. Chem.*, 2009, **694**, 2858–2865.
64 T. Geiger and F. C. Anson, *J. Am. Chem. Soc.*, 1981, **103**, 7489–7496.
65 P. A. Malachesky, L. S. Marcoux and R. N. Adams, *J. Phys. Chem.*, 1966, **70**, 4068–4070.
66 M. D. Ryan, J.-F. Wei, B. A. Feinberg and Y.-K. Lau, *Anal. Biochem.*, 1979, **96**, 326–333.
67 J.-F. Wei and M. D. Ryan, *Anal. Biochem.*, 1980, **106**, 269–277.
68 R. M. Machado and T. W. Chapman, *J. Electrochem. Soc.*, 1987, **134**, 385–391.
69 J. E. Nolan and J. A. Plambeck, *J. Electroanal. Chem.*, 1990, **286**, 1–21.
70 C. C. L. McCrory, C. Uyeda and J. C. Peters, *J. Am. Chem. Soc.*, 2012, **134**, 3164–3170.
71 A. D. Wilson, R. H. Newell, M. J. McNevin, J. T. Muckerman, M. Rakowski DuBois and D. L. DuBois, *J. Am. Chem. Soc.*, 2005, **128**, 358–366.
72 V. Artero, M. Chavarot-Kerlidou and M. Fontecave, *Angew. Chem., Int. Ed.*, 2011, **50**, 7238–7266.
73 X. Hu, B. M. Cossairt, B. S. Brunschwig, N. S. Lewis and J. C. Peters, *Chem. Commun.*, 2005, 4723–4725.
74 H. Cheung, R. S. Tanke and G. P. Torrence, *Ullmann's Encyclopedia of Industrial Chemistry*, Wiley-VCH Verlag GmbH & Co. KGaA, 2000.

